PHYSICAL REVIEW B VOLUME 26, NUMBER 5 1 SEPTEMBER 1982

Raman spectra and lattice dynamics in ferroelectric SbSBr

Takashi Inushima, Kunimitsu Uchinokura, Koya Sasahara, and Etsuyuki Matsuura
Institute of Physics, The University of Tsukuba, Sakura-mura, Ibaraki, 305, Japan
(Received 3 February 1982; revised manuscript received 18 May 1982)

The polarized Raman spectra of SbSBr were measured in both ferro- and paraelectric phases. The frequencies and symmetries of most of the Raman-active phonons in both phases were determined. The Raman data are consistent with the symmetry change from D_{2h}^{16} having 18 Raman-active phonons to C_{2v}^{9} having 33 Raman-active phonons at $T_c = 22.8$ K. The phonons having A_g and B_{1g} symmetries were found to be Davydov pairs with the interaction energy of about 60 cm^{-1}. Based on these results, the lattice dynamics of SbSBr were calculated using a central-force model, which yielded a good fit between the experimental and the calculated phonon frequencies. A strong soft mode with A_1 symmetry appears below T_c. Considering the temperature dependence of its frequency, the absolute scattering efficiency, and the linewidth, the transition is determined to be a displacive one close to the tricritical point. Moreover, in the ferroelectric phase there are two B_1 or B_2 modes, which begin to shift in opposite directions at T_c. By the use of the lattice dynamics of SbSBr, the shifts of these modes are explained by the displacement of Sb and S atoms relative to the Br atom below T_c.

I. INTRODUCTION

Antimony sulfobromide (SbSBr) has an orthorhombic structure of *Pnam* with $a = 8.26$ Å, $b = 9.79$ Å, and $c = 3.97$ Å at room temperature.[1] It shows high photoconductivity[2] and reflectivity.[3] It is a member of V-VI-VII compounds (V=Sb, Bi; VI=S, Se; VII=Cl, Br, I), which have been expected to have both ferroelectric and semiconductive properties.[4] In this group SbSI, SbSBr, BiSI, and BiSBr were reported to show these properties.[5] The existence of ferroelectricity, however, is doubtful in BiSI (Ref. 6) and BiSBr (Ref. 7).

SbSI is the representative of this group and it exhibits anomalous electro-optical and electromechanical properties under visible light illumination,[8] which recently has been a subject of much interest as the cooperative phenomena of the ferroelectric and semiconductive properties.[9]

The transition temperature and the ferroelectric properties of SbSBr had been in confusion. For example, Nitzsche *et al.*[4] and Pikka and Fridkin[5] reported that the transition temperature was near 90 K. In contrast, Furman *et al.* suggested that it was 39 ± 2 K by the Raman scattering measurements of soft phonon in a sample grown by Bridgman method.[10] Recently we found that SbSBr single crystals grown by a vapor-transport method have a phase transition at $T_c = 22.8$ K from the measurements of birefringence.[11] After that we confirmed the existence of the phase transition at that temperature by the measurements of the band-gap energy, the dielectric constant, the spontaneous polarization, and the pyroelectric current.[12] From the results of these experiments, we concluded the following:

(1) The transition is a ferroelectric displacive one and its spontaneous polarization is along the *c* axis, having the Curie-Weiss constant of 7.4×10^4 K, and the spontaneous polarization at 4.2 K is 6.3×10^{-6} C/cm^2.

(2) The band-gap anisotropy of the crystal is not so strong as that of SbSI and its values at room temperature are 2.18 eV for $\vec{E} \perp c$ axis and 2.17 eV for $\vec{E} \| c$ axis ($\vec{E}$ is the polarization vector of light).

(3) The transition is close to the tricritical point.[13] This conclusion was obtained from the results of the critical exponents of birefringence and the temperature dependence of the band-gap energy.[12]

(4) The transition temperature is one of the lowest among the ferroelectrics under a normal condition, which suggests a correlation between the ferroelectric soft mode and the zero-point oscillation of the phonons.[14]

Recently we reported on the polarized Raman spectra of SbSBr single crystals grown by a vapor-transport method[15]; the frequencies and the symmetries of most of the Raman-active phonons in the paraelectric phase were presented. Moreover, there was a ferroelectric soft mode below 22.8 K as was expected from other experiments. In this paper we present the temperature-dependent Raman spectra of SbSBr in both ferro- and paraelectric phases and clarify the changes of the lattice modes which accompany the phase transition.

For the displacive phase transition, all the changes in Raman intensity and frequency are in some way or other related to the change of the structure or the order parameter. In an investigation of the ferroelectric phase transition of SbSI at 290 K it was difficult to establish a correspondence between the lattice modes of the two phases, which makes the nature of the phase transition ambiguous.[16]

The advantage of SbSBr over SbSI for Raman-scattering measurements is its low phase-transition temperature and its transparency to the conventional laser line. Owing to these merits the Raman line shape is sharp and the interference of the second-order Raman lines is prevented. Therefore, it is expected that Raman scattering clarifies the transition mechanism, lattice dynamics, and the space group of ferroelectric phase. It will be shown that the lattice modes consist of Davydov pairs.

As for the lattice dynamics of V-VI-VII compounds, there have been two attempts to analyze the Raman spectra.[7,17] In these cases a simplified unit cell having C_{2h}^2 symmetry was assumed. The assumption, however, does not offer an explanation of the Raman spectra of SbSBr in the paraelectric phase. Another purpose of this paper is to present a model for the lattice dynamics of SbSBr. We take into account the interaction between the double chains as a Davydov splitting and the lattice modes in the double chain are calculated by the use of a central-force model. The results are compared with the experimental results in the paraelectric phase.

Below T_c, we can expect the displacement of atoms accompanied with the condensation of the soft mode. This displacement changes the frequencies of certain normal modes. We present the experimental result of this effect and obtain the consistency between the experimental results and what is expected theoretically.

II. FACTOR-GROUP ANALYSIS

The crystal structure of SbSBr in the paraelectric phase is orthorhombic, belonging to the space group *Pnam* (D_{2h}^{16}) with four molecules (12 atoms) per unit cell.[1] It is shown in the factor-group analysis that SbSBr has 33 optical modes and three acoustic modes. These optical-phonon modes are classified into the following irreducible representations:

$$6A_g+6B_{1g}+3B_{2g}+3B_{3g}$$
$$+3A_u+2B_{1u}+5B_{2u}+5B_{3u} \ .$$

Therefore, in the paraelectric phase, there are 18 Raman-active *gerade* modes and 12 infrared-active *ungerade* modes. The A_u mode is a "silent" one.

The space group of the ferroelectric phase has not been determined yet. According to our investigations on the ferroelectric phase transition of SbSBr, the transition is close to tricritical point and the spontaneous polarization appears along the c axis.[12] In this case, by the group-theoretical analysis using Landau's theory of the second-order phase transition, the ferroelectric phase is determined to be orthorhombic $Pna2_1$ (C_{2v}^9) with four molecules per unit cell, which is the same as that of SbSI.[18] This phase has 33 optical phonons, all of which are Raman-active modes having the symmetries of

$$8A_1+9A_2+8B_1+8B_2 \ .$$

Among them, A_2 modes are infrared inactive.

According to Loudon[19] these modes have the following Raman tensors,

$$A_g,A_1\colon \begin{bmatrix} a & & \\ & b & \\ & & c \end{bmatrix} ,$$

$$B_{1g},A_2\colon \begin{bmatrix} & d & \\ d & & \\ & & \end{bmatrix} ,$$

$$B_{2g},B_1\colon \begin{bmatrix} & & e \\ & & \\ e & & \end{bmatrix} ,$$

$$B_{3g},B_2\colon \begin{bmatrix} & & \\ & & f \\ & f & \end{bmatrix} .$$

These matrices are constructed with respect to the crystal a, b, and c axes. The correlation diagram of the symmetry change is given in Fig. 2 of Ref. 16.

In the interpretation of the infrared transmission and the Raman scattering spectra of group V-VI-VII compounds many authors have used the simplified structure having only two molecules per unit cell.[20] That is, the crystal is composed of two double chains with strong interaction between the Sb atoms of one chain and the S atoms of the other, and the interaction between different double chains is neglected. In Fig. 1 of Ref. 1, the simplified unit cell is composed of the Sb(3)S(4)Br(1) chain and the

Sb(4)S(3)Br(2) chain.[21] In this case the space group of SbSBr in the paraelectric phase is $P2_1/m$ (C_{2h}^2) and it is $P2_1$ (C_2^2) in the ferroelectric phase. In the simplified structure, there are fifteen optical modes and three acoustic modes. In the paraelectric phase, optical-phonon modes are classified as follows,

$$6A_g + 3B_g + 2A_u + 4B_u \ .$$

Therefore, we see nine Raman-active *gerade* modes in the paraelectric phase, but one of the A_g modes is a rotational mode and its frequency should be zero in this model. In the ferroelectric phase all the optical modes become Raman active,

$$8A + 7B \ .$$

The corresponding Raman tensors are

$$A_g,A: \begin{bmatrix} a & d & \\ d & b & \\ & & c \end{bmatrix} ,$$

$$B_g,B: \begin{bmatrix} & & e \\ & & f \\ e & f & \end{bmatrix} .$$

The correlation diagram of the simplified unit cell is also listed in Fig. 2 of Ref. 16.

III. EXPERIMENTAL PROCEDURE

The single crystals used in the Raman-scattering measurements were grown by a vapor-transport method. The details were reported previously.[11] The crystals are needlelike and 30 to 40 mm in length along the c axis. The crystals have several natural faces with high reflectivity, which are 0.6–0.8 mm in width. The orientation of the crystal was determined by measuring the angles between the faces. The main flat plane was (110).

The Raman spectra were obtained by a 6328-Å line of He-Ne laser and a Spex double monochromator. The band-gap energy of this material is about 2.18 eV at room temperature. Thus the sample is transparent to the laser light in the temperature region investigated. The laser intensity was reduced to about 4 mW for the measurements of the soft phonon. A Spex third monochromator was also used to get pure spectra. For the detection we used the combination of an RCA 31034 photomultiplier tube and a synchronous single-photon counting system. The spectral resolution was 0.5 cm^{-1}. To examine the temperature dependence of the Raman spectra of certain modes, we used a multichannel detector (IDARSS) of Tracor Northern.

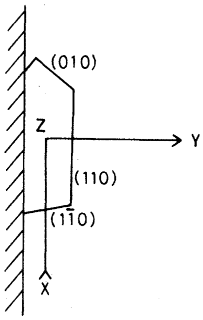

FIG. 1. Raman scattering geometry in this experiment. The crystal faces are shown in the figure. The propagating directions of light are expressed as X and Y. The crystal c axis is perpendicular to the figure and parallel to Z. The crystal shape is a typical one and the interchange of its a and b axes does not produce meaningful difference in the Raman spectra.

Figure 1 shows the experimental arrangement for the polarized Raman scattering measurement. The Z direction is chosen to the crystal c axis and the Y direction to be perpendicular to (110). At this geometry the measured Raman-active modes in the $X(ZZ)Y$, $X(YX)Y$, and $X(ZX)Y$ configurations correspond to the representations of $A_g(A_1)$, $A_g(A_1)+B_{1g}(A_2)$, and $B_{2g}(B_1)+B_{3g}(B_2)$, respectively. The sample is attached to a copper block in a vacuum cryostat with GE Varnish 7031. Both ends of the sample were electrically short-circuited with silver paste. This procedure to prevent the occurrence of space charge is important in the case of SbSBr. SbSBr shows high photoconductivity[2] and its transition temperature is very low. Therefore, under visible laser-light illumination, the occurrence of space charge is unavoidable, which makes the transition temperature ambiguous.

The temperature was monitored by a gold-iron-chromel thermocouple mounted near the sample. It was also monitored by the intensity ratio of the Stokes to anti-Stokes line of the soft mode. The temperature was controlled within 0.1 K.

IV. RESULTS

A. Paraelectric phase

The Raman spectra of SbSBr were measured over the temperature range from 7 to 300 K in the frequency range from 3 to 350 cm^{-1} for various orientations. Figure 2 shows the Raman spectra at 300 K for the three configurations of $X(YX)Y$, $X(ZZ)Y$, and $X(ZX)Y$. In the $X(YX)Y$ configuration nine phonons are observed clearly, that is, 47,

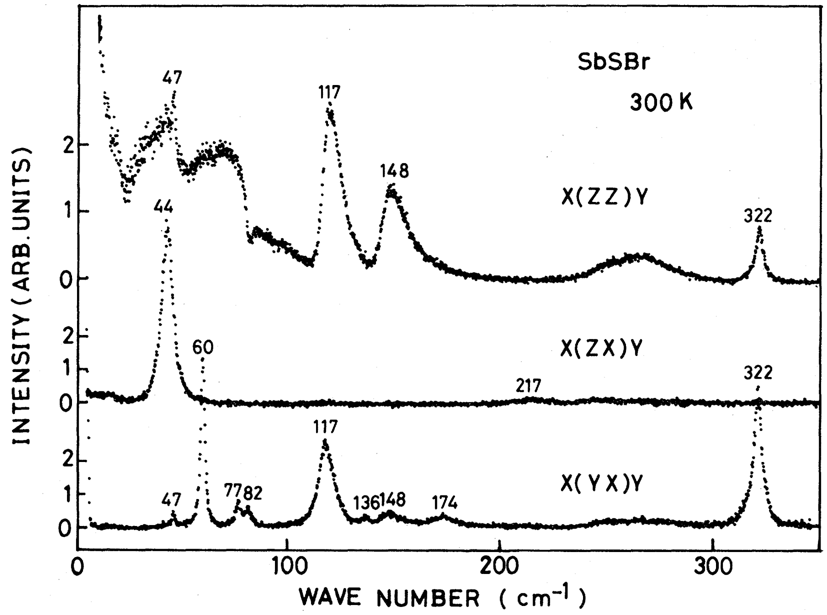

FIG. 2. Raman spectra of paraelectric SbSBr at 300 K. Second-order spectra exist below 85 cm^{-1} in $X(ZZ)Y$ and their intensities decrease as the temperature decreases. The peak at 322 cm^{-1} consists of three peaks in the paraelectric phase (see Fig. 1 of Ref. 15).

60, 77, 82, 117, 136, 148, 174, and 322 cm^{-1}. The phonon at 322 cm^{-1} is observed as a single peak at 300 K but it is resolved distinctly as three peaks below 200 K and they are 317, 323, and 328 cm^{-1} at 40 K (see Fig. 1 of Ref. 15). Near 260 cm^{-1} there is a broad band, which remains broad but gradually increases its intensity as the temperature is lowered.

In $X(ZZ)Y$ configuration four phonons are observed, that is, 47, 117, 148, and 322 cm^{-1}. The intensity of the phonon at 47 cm^{-1} is very weak at low temperature but it increases with increasing temperature. The phonon at 322 cm^{-1} consists of two phonons which exist at 317 and 323 cm^{-1} at 40 K. They are observed as separate lines below 100 K, but the intensity of 317 cm^{-1} is weak. There is a broad band near 260 cm^{-1} and its intensity increases as the temperature decreases. The halfwidth of the line, however, remains broad in the paraelectric phase. The Raman spectra below 85 cm^{-1} is probably a second-order one, and its intensity increases as the temperature increases. The maximum intensities of the second-order one are obtained at 50 and 70 cm^{-1}. When the temperature is low, the phonon of 60 cm^{-1} becomes observable.

In the $X(ZX)Y$ configuration there are one strong line at 44 cm^{-1} and two broad bands around 217 and 260 cm^{-1}. As the temperature decreases, the band around 260 cm^{-1} disappears. On the other hand, the band around 217 cm^{-1} becomes sharp and strong. No other line is observed in the paraelectric phase.

In $X(ZX)Y$ configuration we see only the TO mode because the scattering plane is perpendicular to the c axis and the B_{2g} and B_{3g} modes observed in this configuration are vibrating along the c axis.

As was mentioned in Sec. II, the simplified crystal structure of C_{2h}^2 having two molecules per unit cell, which has been used in SbSI, is not adequate for SbSBr because there are more than five A_g modes, which is the maximum A_g phonon number in the simplified unit-cell model. So far there have been two reports on the Raman spectra of SbSBr. One was presented by Teng *et al.*[22] and the other was reported by Furman *et al.*[10] The former did the experiment at room temperature with unpolarized light. The latter used the sample grown by the Bridgman method. Both of them reported less than nine Raman-active phonons at room temperature and a close resemblance of the Raman spectra between SbSI and SbSBr. This is true when the experimental resolution is insufficient and at room temperature. But the discrepancy is evident in the spectra at 40 K.[15] Furman *et al.* reported as follows: (a) The phonon at 263 cm^{-1} is a $B_g(C_{2h}^2)$ mode (in our data it corresponds to 260-cm^{-1} mode). (b) A

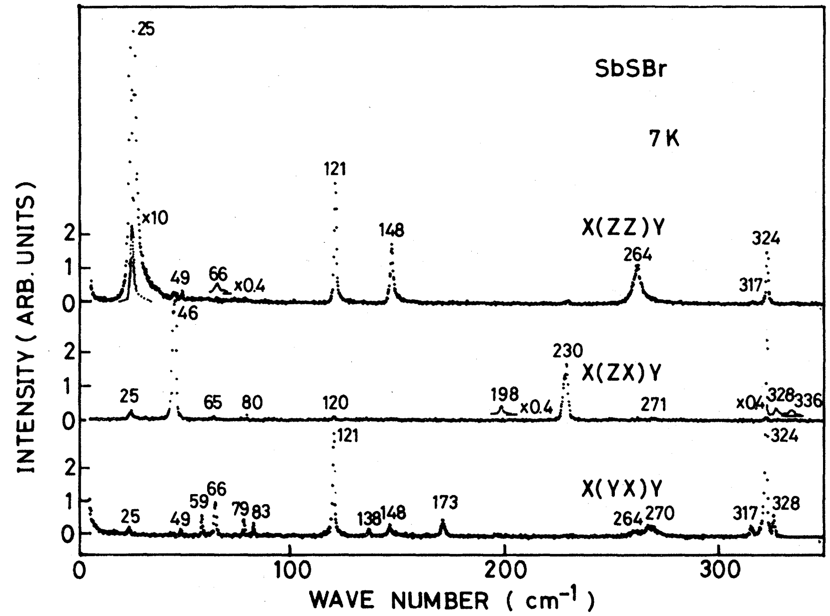

FIG. 3. Raman spectra of ferroelectric SbSBr at 7 K. The existence of the weak peak was confirmed using a multichannel detector. The phonon at 25 cm^{-1} is a soft mode and its temperature dependence is given in Fig. 2 of Ref. 15.

soft mode was found to condense at 39±2 K with the temperature dependence of the frequency of $(T_c-T)^{0.30}$. (c) The soft mode was found to be coupled to a higher-frequency mode at 42 cm^{-1}. We will show in later sections that their results (a) and (c) are quite different from our results. As for (b), we have discussed the discrepancy between their T_c and ours in a previous paper,[11] and for the soft mode our results are given in Sec. IV C.

B. Ferroelectric phase

The polarized Raman spectra in the ferroelectric phase at 7 K are shown in Fig. 3. In the $X(YX)Y$ configuration, all of the 11 paraelectric modes were observed at this temperature. Four additional lines were observed at 25, 59, 264, and 270 cm^{-1}. The phonons at 59 and 270 cm^{-1} are apparently A_2 modes which were not observed in the $X(ZZ)Y$ configuration. These phonons gradually increase their intensity as the temperature lowers from T_c. Other phonons at 25 and 264 cm^{-1} are A_1 modes which are more strongly observed in $X(ZZ)Y$ configuration.

In the $X(ZZ)Y$ configuration there are two modes which show strong temperature dependence in the ferroelectric phase, at 25 and 264 cm^{-1}. The phonon at 25 cm^{-1} is a ferroelectric soft mode as will be shown in the next section. The temperature-dependent spectra near 264 cm^{-1} are shown in Fig. 4, which were obtained by a multichannel detector. The spectrum at 264 cm^{-1} drastically changes near 22.8 K. At this temperature the halfwidth of the phonon becomes narrower, to be one-third of that in the paraelectric phase. At the same time the broad band in $X(YX)Y$ symmetry

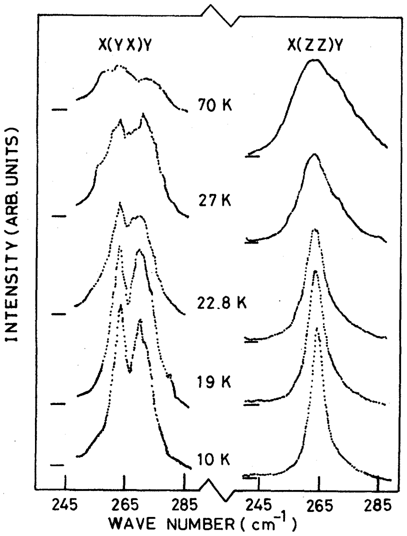

FIG. 4. Temperature-dependent Raman spectra of 264-cm^{-1} A_1 and 270-cm^{-1} A_2 modes in SbSBr near $T_c=22.8$ K. These spectra were not observed in the $X(ZX)Y$ configuration. The Raman intensity is about 4 times stronger in $X(ZZ)Y$ than in $X(YX)Y$.

becomes sharper and stronger and is clearly resolved into two peaks (264 and 270 cm^{-1}). In the $X(ZX)Y$ configuration such a band was not observed.

In $\vec{E}\|c$ axis configuration there are two B_{1u} modes in the paraelectric phase, which become Raman-active A_1 modes below T_c. One is a ferroelectric soft mode as observed at 25 cm^{-1}. Then we assigned the mode at 264 cm^{-1} to another infrared-active $B_{1u}(A_1)$ mode. The A_2 mode at 270 cm^{-1} is a silent A_u mode above T_c, which is accompanied with a 264-cm^{-1} B_{1u} mode (see Sec. V A). As seen in Figs. 2 and 4, this broad band is observed even in the paraelectric phase. This suggests that there are impurities or lattice imperfections in the crystal, which makes the Raman-inactive mode active above T_c. It is reported on SbSI that some Raman-active modes were observed in the infrared spectrum above T_c.[23]

Furman *et al.* reported the drastic intensity change of the modes at 225 and 264 cm^{-1} (which corresponds to 230 and 264 cm^{-1} in our experiment) below T_c. This is true for 264-cm^{-1} mode, though they assigned this mode to $B(C_{2h}^2)$ symmetry, but the intensity of 230-cm^{-1} mode is nearly constant below T_c. The reason why Furman *et al.* assigned the 264-cm^{-1} mode to the $B(C_{2h}^2)$ mode is that the corresponding mode of SbSI was assigned to B symmetry.[16] We suppose from the result of SbSBr that 239-cm^{-1} mode of SbSI might be an A_1 mode as was assigned by Balkanski *et al.*[17] Furman *et al.* reported the temperature dependence of the frequency of 42-cm^{-1} mode below T_c which is similar to Fig. 5. They assigned the dependence to the interaction with soft A_1 mode. This mechanism is impossible in pure and perfect samples from the symmetry consideration. Their result indicates that the symmetry of their sample is low due to imperfections and therefore the mode is coupled with the soft mode.

In the $X(ZX)Y$ configuration ten phonon lines were observed in the ferroelectric phase, that is, 25, 46, 65, 80, 120, 198, 230, 271, 328, and 336 cm^{-1}. The lines at 46 and 230 cm^{-1} are paraelectric modes. Other lines are weak, some of which have the frequencies similar to those of other symmetry phonons. These lines, however, are observed only in the ferroelectric phase. As seen in Sec. II, 16 phonons are expected to be observed in the ferroelectric phase in this configuration. As seen in Fig. 3 the intensity of the phonons except at 46 and 230 cm^{-1} is so weak that we could not assign strictly the symmetry of most of the phonons. The phonons at 46 and 230 cm^{-1} shift to opposite directions below T_c as shown in Fig. 5. The temperature where the peaks begin to shift is 22.8±0.3 K, which is the phase-transition temperature. The temperature variations of these modes ($\Delta\omega$) are expressed as follows,

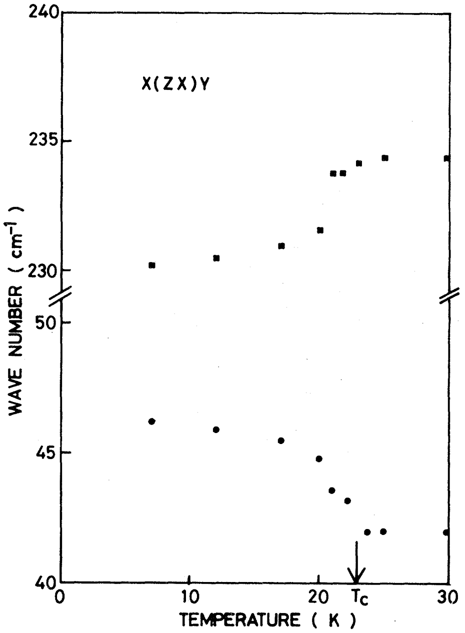

FIG. 5. Temperature-dependent frequencies of 46- and 230-cm^{-1} modes near $T_c=22.8$ K. These modes have a B_1 or B_2 symmetry and their frequencies have a temperature dependence expressed by Eq. (1).

$$\Delta\omega \simeq \pm 6.5\left[\frac{T_c-T}{T_c}\right]^{0.5}, \tag{1}$$

in units of cm^{-1} where plus and minus signs correspond to 46- and 230-cm^{-1} modes, respectively. As will be discussed in Sec. V C, the feature shown in Fig. 5 is a reliable evidence of the displacive ferroelectric transition in SbSBr.

C. Soft mode

Recently we reported the existence of the A_1 soft mode in SbSBr below 22.8 K (see Fig. 2 of Ref. 15). There we saw that the line shape of the soft mode is expressed by a single damped harmonic oscillator model, because there is no phonon to be coupled near the soft mode. The line-shape function was given as follows:

$$g(\omega)=\left[\frac{1}{\exp(\hbar\omega/kT)-1}+1\right] \times\frac{\gamma_s\omega}{(\omega_s^2-\omega^2)^2+\gamma_s^2\omega^2}, \tag{2}$$

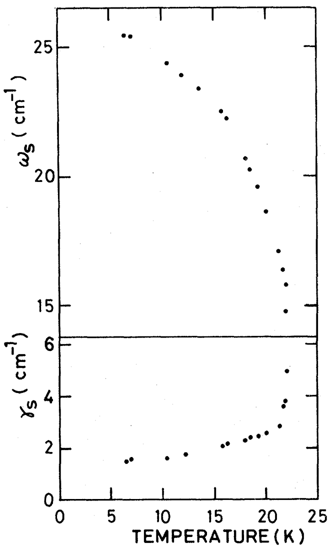

FIG. 6. Temperature dependences of the frequency ω_s and the damping factor γ_s of the A_1 soft mode below T_c.

where γ_s and ω_s are the damping factor and the frequency of the soft mode, respectively. Using Eq. (2) we show the temperature dependence of the soft-mode frequency ω_s and the damping factor γ_s in Fig. 6.

The transition temperature of SbSBr is not clearly determined from Fig. 6, owing to the decrease of the intensity of the soft mode near T_c. It is, however, determined to be 22.8 ± 0.3 K from Fig. 5 where the B_1 or B_2 mode begins to shift. The value is reasonable when we compare it with those obtained from other experimental techniques.[12] Using this T_c, and by plotting the frequency versus $\epsilon = (T_c - T)/T_c$ on a log-log plot, we find that the frequency decreases toward zero at nearly $\frac{1}{4}$ power of ϵ, that is,

$$\omega_s = 27.8 \times \epsilon^{0.23} \ , \quad T_c = 22.8 \ , \quad \epsilon < 0.1 \ , \tag{3}$$

where ω_s is in cm^{-1} and T_c in K. The temperature dependence of the soft-mode frequency is related to the static susceptibility $\chi_0(T)$ as

$$\chi_0(T) \propto \omega_s^{-2} \ , \tag{4}$$

and the critical exponent γ is defined as

$$\chi_0(T) \propto \epsilon^{-\gamma} \ . \tag{5}$$

Therefore, Eq. (3) gives the critical exponent $\gamma/2 = 0.23$ for the soft mode, which is much smaller than 0.5 of the classical value. The various models for describing the phase transition give exponent γ's larger than unity and it is impossible to explain such a small value of γ.

In SrTiO$_3$, Steigmeier and Auderset revealed that the soft-mode frequency is proportional to the order parameter.[24] If this relation holds also in SbSBr, the temperature dependence of ω_s gives the critical exponent β and $\beta = 0.23$ is expected from the Landau theory when the transition is close to the tricritical point ($\beta = \frac{1}{4}$).

Previously we reported that the critical exponent β obtained by the measurement of the birefringence is 0.26.[12] Moreover from the temperature dependence of the band-gap energy, we obtained $\beta = 0.26$ in the ferroelectric phase. There is little difference between the exponent obtained in Eq. (3) and those reported previously. Therefore, the soft-mode frequency probably depends linearly on the order parameter in SbSBr. This fact may be explained in terms of a precursor order parameter of the low-temperature phase transition.[25]

The damping factor γ_s increases rapidly near T_c and has a tendency to diverge at T_c. Actually such a divergence is expected in the vicinity of structural phase transitions. The population factor of the soft mode increases rapidly where $\hbar\omega_s \ll kT$ is satisfied. Therefore, soft-phonon relaxation increases near T_c and has a nature to diverge at T_c.[26]

As is seen in Fig. 2 of Ref. 15, the Rayleigh component does not seem to depend much on temperature below and above T_c and the soft mode seems to disappear near T_c. In order to see this feature we plot the experimentally integrated intensity of the soft phonon against T in Fig. 7. The intensity was obtained by integrating the intensity of the Raman

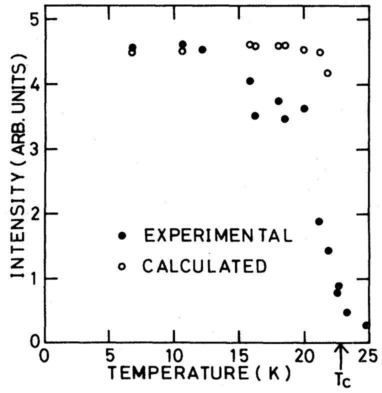

FIG. 7. Temperature-dependent Raman intensity of the soft mode near T_c. The calculated values in the figure were obtained from Eq. (6) using the experimentally obtained ω_s and γ_s of Fig. 6. Intensities are normalized at 12 K.

spectra from 3 to 30 cm^{-1}. It is clear from Fig. 7 that below 15 K the intensity is almost constant, but near T_c it decreases to zero as the temperature increases. Theoretically the integrated intensity $S(T)$ of the soft mode corresponding to the experimentally integrated intensity is written as

$$S(T)=A\,|\alpha_{zz}|^2\int_{3\ \mathrm{cm}^{-1}}^{30\ \mathrm{cm}^{-1}} g(\omega)d\omega\ , \tag{6}$$

where A is a constant and α_{zz} is the derivative of the optical polarizability per unit volume with respect to the soft-mode displacement in this configuration. $g(\omega)$ is given in Eq. (2). As the soft mode is Raman inactive above T_c, α_{zz} is proportional to the order parameter below T_c. From the results of other experiments, $\alpha_{zz}\propto(T_c-T)^{1/4}$ is expected. Using this relation and ω_s and γ_s of Fig. 6, we calculated $S(T)$ and plotted it in Fig. 7. It should be noted that in the course of calculation of Eq. (6) we cannot use the approximation $kT \gg \hbar\omega_s$ because T_c of SbSBr is low. As seen in Fig. 7, $S(T)$ is nearly constant below T_c while experimental value is not. The difference may have come from the lack of the integration of the central component. The coexistence of para- and ferroelectric phases near T_c does not contribute to this decrease of the intensity because the intensities of other Raman-active phonons do not change during the phase transition.

The result of Raman scattering measurements of the soft mode shows that the phase transition is caused by the lattice instability. This conclusion agrees with the fact that SbSBr has the large Curie-Weiss constant expected for the material which shows the displacive phase transition.[12]

V. DISCUSSIONS

A. Lattice-mode assignment

In Fig. 2 we saw far more Raman-active phonons in paraelectric SbSBr than those expected from the simplified unit-cell model which was applicable to SbSI and so on. In Table I we compile the paraelectric and ferroelectric mode frequencies at 300 and 7 K. In spite of this fact, there is close resemblance between the Raman spectra of SbSI and SbSBr as has been suggested by Teng *et al.*[22] and Furman *et al.*[10] This result indicates that the Raman spectra of SbSBr is mainly governed by C_{2h}^2 symmetry and the interaction between the double chains can be taken into account as a perturbation. This interaction gives rise to mode splitting.

In the following analysis we used the approximation that the phonon spectra are mainly governed by a double-chain symmetry and the interaction is introduced by the crystallization of the double chain (factor-group splitting or Davydov splitting). When we consider the modes of a double chain (simplified unit-cell model) compared with those of crystalline (full space group) SbSBr, the following differences are to be noted: (1) All of the double-chain modes are split into two components in the crystal. (2) A rotational mode of frequency zero in a double chain becomes two Raman-active modes with finite frequencies in the crystal. The frequencies give the magnitude of the interaction between the double chains when they rotate along the c axis. (3) Three lattice modes of B_{2u}, B_{3u}, and A_u appear in the crystal. These modes are expected to have low frequencies, which give the magnitude of the interaction between the double chains when they move rigidly in opposite directions along a, b and c axes, respectively. Thus they have a nature of so-called "rigid-chain" mode in low-dimensional materials[27] and are the Davydov pairs to the acoustic modes.

In this model A_g as well as B_g of C_{2h}^2 have a relation as follows[28]:

$$\omega_u^2-\omega_v^2=\omega_I^2\ , \tag{7}$$

where ω_I is the interaction energy between the double chains and u and v are the Davydov pairs shown in Table I. We examine the validity of the equation in Table I using the frequencies of A_1 and A_2 at 7 K. In this model A_1 and A_2 are the in-phase and out-of-phase motion of the A (C_{2h}^2) mode, respectively. Hence we chose the A_2 mode having nearly equal but slightly higher frequencies than A_1. Equation (7) gives ω_I in all the A (C_{2h}^2) modes which vibrate in the a-b plane, within 60 ± 10 cm^{-1} except at 148 cm^{-1}. One A_2 mode is considered to be at 324 cm^{-1}, which is accidentally overlapped by the 324-cm^{-1} A_1 phonon.

In the paraelectric D_{2h}^{16} phase there are three silent modes having A_u symmetry, which become Raman-active A_2 modes in the ferroelectric C_{2v}^9 phase. Two of them are the out-of-phase motion of the infrared-active modes and the other one is the mode which is the out-of-phase motion of the acoustic mode (rigid-chain mode). These modes vibrate along the c axis. From Fig. 3 frequencies of the A_2 modes observed only below T_c are 59 and 270 cm^{-1}. In Fig. 4 we saw that the 270-cm^{-1} mode is the A_2 Davydov pair to the 264-cm^{-1} A_1 mode. From Eq. (7) this pair has $\omega_I=57$ cm^{-1}, which is close to the 59-cm^{-1} A_2 mode. Then we assign the "rigid-chain" mode as 59 cm^{-1}, which gives the interaction energy between the double chains when they vibrate along the c axis.

As for the B_{2g} (B_1) and B_{3g} (B_2) modes we did

TABLE I. Observed frequencies of SbSBr and its Davydov pairs[b] together with their interaction energy ω_I. ω_I is obtained from *Eq.* (7).

Paraelectric phase (300 K)			Ferroelectric phase (7 K)		
Symmetry	Frequency (cm^{-1})	Mode[a]	Symmetry	Frequency (cm^{-1})	ω_I (cm^{-1})
A_g	47	A_g^2	A_1	49	62.0
B_{1g}	77		A_2	79	
A_g	60	A_g^1	A_1	66	50.3
B_{1g}	82		A_2	83	
A_g	117	A_g^3	A_1	121	66.4
B_{1g}	136		A_2	138	
A_g	148	A_g^4	A_1	148	89.6
B_{1g}	174		A_2	173	
A_g	*	A_g^5	A_1	317	67.0
B_{1g}	*		A_2	324	
A_g	322	A_g^6	A_1	324	51.1
B_{1g}	*		A_2	328	
B_{1u}		A_u^2	A_1	25	soft mode
A_u			A_2	*	
B_{1u}		A_u^3	A_1	264	56.6
A_u			A_2	270	
A_u			A_2	59	rigid-chain mode
B_{2g} or B_{3g}	44	B_g^1	B_1 or B_2	46	
B_{2g} or B_{3g}	217	B_g^3	B_1 or B_2	230	
B_{2u} or B_{3u}			B_1 or B_2	25	
B_{2u} or B_{3u}			B_1 or B_2	65	
B_{2u} or B_{3u}			B_1 or B_2	80	
B_{2u} or B_{3u}			B_1 or B_2	120	
B_{2u} or B_{3u}		B_u^4	B_1 or B_2	198	
B_{2u} or B_{3u}			B_1 or B_2	271	
B_{2u} or B_{3u}			B_1 or B_2	328	
B_{2u} or B_{3u}		B_u^6	B_1 or B_2	336	

[a] Phonons used to calculate Table II. Their notations are given in Fig. 9.

[b] In the simplified unit-cell model, Davydov pairs are obtained from the following relations: $A_g \rightarrow A_g + B_{1g}$; $A_u \rightarrow A_u + B_{1u}$; $B_g \rightarrow B_{2g} + B_{3g}$; $B_u \rightarrow B_{2u} + B_{3u}$ in the paraelectric phase and $A \rightarrow A_1 + A_2$ and $B \rightarrow B_1 + B_2$ in the ferroelectric phase.

not observe such a splitting owing to poor scattering intensity.

From the consideration above we see that the splitting energy is almost independent of the particular mode in A (C_{2h}^2) symmetry. This suggests that the interaction energy between the double chains are about 60 cm^{-1} and the interaction between the double chains is isotropic in SbSBr. In Table I, one of the A (C_{2h}^2) modes is a rotational mode, which must have a similar frequency to the interaction energy. Then we assigned it to the 66- and 83-cm^{-1} pair. We will see in the next section that this choice is reasonable.

The phonon assignment above is based on the assumption that the ferroelectric phase is C_{2v}^9. This assumption comes from the fact that the phase transition is close to the tricritical point and the spontaneous polarization appears along the c axis. In the analysis of our Raman spectra we found no contradiction to this assumption.

B. Lattice dynamics in SbSBr

As was mentioned in the previous sections, most of the lattice modes in SbSBr were observed in the Raman spectra and the interaction between the double chains produces the Davydov pairs in these modes. This reveals that the lattice dynamics in SbSBr can be calculated using the simplified unit-cell model. In this section we calculate the normal modes in SbSBr by the use of Born—von Kármán model, and in the next section we see the effect of the phase transition on these normal modes considering the long-range Coulomb force.

The lattice dynamics of V-VI-VII compounds were treated by Furman *et al.*[7] They assumed the noninteracting double-chain model and the double-chain modes were solved by an axially symmetric model. They use the three shortest bondings in the double chain and each bonding has stretching force and axially symmetric bending force. But in the course of the calculation we found out that there was a pitfall in their treatment. They neglected the rotational symmetry of the chain. In principle, rotational displacement receives no restoring force, therefore it has zero frequency and its symmetry is totally symmetric. Their solutions do not have a rotational mode with frequency zero. This is quite an important error in the calculation of the vibration of a chain. We performed the calculation based on their model by taking into account the rotational symmetry. Then we found out that all the bending forces must be zero and other zero frequency modes appeared. Without bending forces the rotation of bromine around the *c* axis has no restoring force. Therefore, the chain is unstable in this mode, and the model itself is completely meaningless. Therefore, a different model must be used.

We calculate the lattice dynamics of SbSBr by the use of the following two approximations.

(1) The interchain interaction is so weak that all the modes are considered within the framework of Davydov splitting. Then the double-chain model having the space group C_{2h}^2 is sufficient to determine the lattice vibration.

(2) Lattice potential is expressed by the central-force model in which we take into account up to the fifth nearest-neighbor interaction in a double chain.

Usually for molecules and in this case for chain, the valence-force model is used. But for our double chain we probably need 15 independent force constants. Fitting this model to the experimental results seems meaningless, because too many parameters are involved. Therefore, we choose the axially symmetric mode, adding other bondings between sulfur and bromine and between antimony and antimony to those used in Ref. 7. These bondings are shown in Fig. 8 and are necessary to stabilize the chain, and they must be considered to supplement the bending forces of the valence-force model. In this model when we consider rotational symmetry, all the bending forces are again zero, and the axially symmetric model becomes the central-force model.

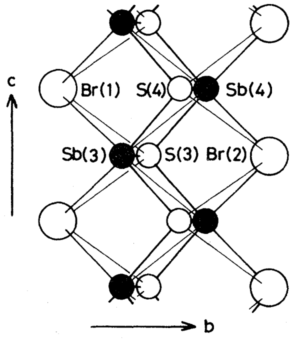

FIG. 8. Bondings used for the calculation of the lattice dynamics of SbSBr in the paraelectric phase. The figure is the projection of the structure on the (100) plane. The unit cell is composed of two chains of Sb(3)S(4)Br(1) and Sb(4)S(3)Br(2) and has a symmetry of C_{2h}.

In the central-force model, the force constants have the form

$$\phi_{\alpha\beta}(ll',jj')=(R_\alpha R_\beta/|R|^2)F_{jj'}\ , \tag{8}$$

where $\phi_{\alpha\beta}(ll',jj')$ is the $\alpha\beta$ Cartesian component of the force constant between the atoms j and j' in l and l' unit cells. R_α is the α Cartesian component of the bond length R. F is so-called bond stretching force. Considering only long-wavelength modes and $L=l-l'$, the diagonalization of the dynamical matrix of

$$D_{\alpha\beta}(k,jj')=\sum_L \phi_{\alpha\beta}(L,jj')(M_jM_{j'})^{-1/2}e^{ikR_L} \tag{9}$$

gives 18 phonon frequencies. From symmetry considerations this matrix divides into two blocks, a 12×12 block which represents vibrations in the *a-b* plane and a 6×6 block which represents the vibrations along the *c* axis.

For the summation in Eq. (9), we used the bondings shown in Fig. 8 which give us five fitting parameters. At least five bondings are necessary to obtain a conclusive result.

For the determination of the most appropriate force constants, we solved the dynamical matrix by the methods which are described in Ref. 29. For the lattice parameters we used the x-ray data of Christofferson and McCullough.[1] For the construction of the weighted frequency matrix, we used the frequencies of five A_g modes and two B_{2g} or B_{3g} modes at T_c. For the zero-frequency rotational mode we chose the A_g mode of 66 cm^{-1}. Choosing another mode makes it difficult to fit the experimental values in low-frequency modes. For the B_u phonon frequencies we used two B_2 modes of 198 and 336 cm^{-1} and for the A_u phonon we used 264 cm^{-1}. They are the three most reliable modes in Table I, which become Raman active in the ferroelectric phase.

The fit between calculated frequencies and the experimentally obtained ones is listed in Table II, and the resulting set of parameters is given in Table III. A representative set of eigenvectors is shown in Fig. 9. In the figure A_u^1, B_u^1, and B_u^2 are the acoustic modes. A_g^1 is the rotational mode of frequency zero. A_u^2 is the ferroelectric soft mode.

The above calculation agrees well with experimental results and the restricted input data seem to be sufficient to determine the force constants. As shown in Table III the force constants between Sb and S are far stronger than those of other bondings. This result indicates that the lattice of SbSBr is constructed mainly of Sb-S chains along the *c* axis and one chain is tightly linked to another chain by Sb—S bonding in the *a*-*b* plane. It should be noted that the force between S(3) and Br(1) determines the frequencies of A_g^2, B_g^1, and B_u^3 dominantly. These frequencies are about 50 cm^{-1}. The distance between S(3) and Br(1) is 3.58 Å. The shortest bonding between the two double chains exists at S(2)—Br(1) or S(1)—Br(2) of Fig. 1 of Ref. 1 and the distance is 3.46 Å.[21] Therefore, Br(1) is expected to receive the force from S(3) similar to the force from S(2). The fact that the frequencies of the rotational mode (65 cm^{-1}), Davydov splitting energy (60 cm^{-1}), and rigid-chain mode (59 cm^{-1}) are nearly equal to those of A_g^2, B_g^1, and B_u^3 suggests that the Br atom in SbSBr works to bond the Sb-S chains and stabilize the crystallization of SbSBr. The results given in Fig. 9 represent the chain vibration of SbSBr. The results obtained by Furman *et al.* are quite different from Fig. 9 in low-frequency parts of *a*-*b* plane vibration. Especially the frequency of A_g^1 of Fig. 9 (rotational mode) should be zero regardless of the force constants. No

TABLE II. Observed and calculated frequencies of phonons of SbSBr (cm^{-1}).

Mode[a]	Obs.[b]	Calc.	Symmetry[d]
A_g^1	66	0[c]	A_g
A_g^2	49	55	A_g
A_g^3	121	125	A_g
A_g^4	148	150	A_g
A_g^5	317	270	A_g
A_g^6	324	320	A_g
A_u^2	25[e]	125	B_{1u}
A_u^3	264	255	B_{1u}
B_g^1	42	50	B_{2g} or B_{3g}
B_g^2		135	B_{2g} or B_{3g}
B_g^3	234	260	B_{2g} or B_{3g}
B_u^3		45	B_{2u} or B_{3u}
B_u^4		135	B_{2u} or B_{3u}
B_u^5	198	225	B_{2u} or B_{3u}
B_u^6	336	310	B_{2u} or B_{3u}

[a] Mode is given in Fig. 9.

[b] Frequencies are obtained at T_c (22.8 K).

[c] Rotational mode.

[d] For the *ungerade* mode frequencies we used A_1 (A_2) and B_1 (B_2) symmetry phonon frequencies at 7 K, where they become Raman active and their frequencies show little temperature dependence. Soft-mode frequency was not used for calculation.

[e] Soft mode.

TABLE III. Force constants for various bonds (10^4 dyn/cm).

$F_{\text{Sb(3)-Br(1)}} = 5.1$
$F_{\text{Sb(3)-S(4)}} = 8.3$
$F_{\text{Sb(3)-S(3)}} = 13.8$
$F_{\text{S(3)-Br(1)}} = 0.4$
$F_{\text{Sb(3)-Sb(4)}} = 9.5$

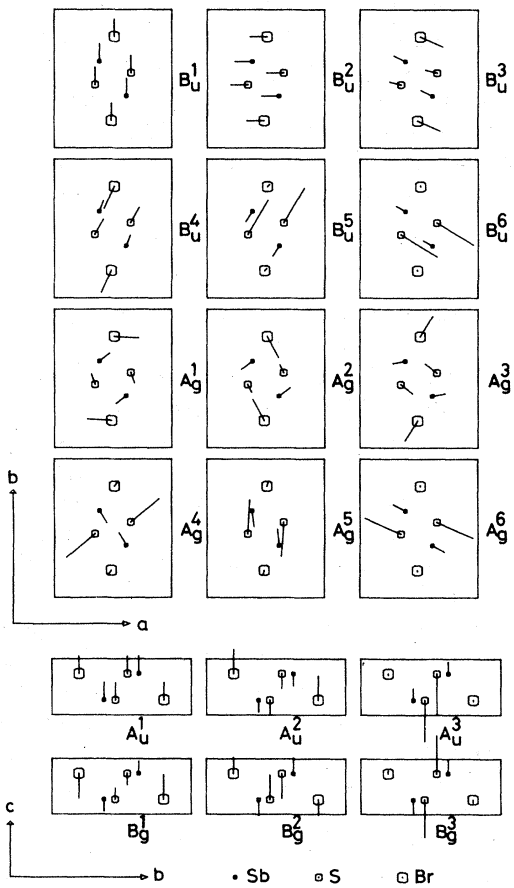

FIG. 9. Projections of the calculated eigenvectors for each mode of the lattice vibration. The eigenvector is transformed to the atomic displacement. The magnitude of the displacement is exaggerated. The superscript of a symmetry is arranged in the order of frequency.

such mode exists in Fig. 4 of Ref. 7. This is because their model is not appropriate in A_g (C_{2h}^2) modes. The modes obtained by them are not the eigenfunctions of the vibration of the double chain.

This model is applicable not only to SbSBr but to other V-VI-VII compounds, especially to SbSI. The remarkable similarity between the Raman spectra of SbSI and SbSBr is caused from the fact that the force constants related to the Br atom are far weaker than those between the Sb and S atoms. For example, the modes of A_g^6 and B_u^6, which show the highest frequencies in Raman-active and infrared-active phonons, respectively, are expected to be insensitive to the replacement of Br with I atoms. In fact in SbSI, the highest frequency was obtained experimentally at 319 cm^{-1} for the Raman-active mode and at 330 cm^{-1} for the infrared-active mode.[16] In SbSBr 324 and 336 cm^{-1} are obtained for these modes, respectively. In the Raman spectra of SbSI, there seems to be no "rigid-chain" mode. As the shortest distance between the two double chains is 3.61 Å (in SbSBr, 3.46 Å) and the anisotropy in many physical quantities is much larger than that of SbSBr, the interchain interaction is expected to be weaker than that of SbSBr.[12] Then we expect that the rigid-chain mode and rotational mode must be far smaller than the 60 cm^{-1} of SbSBr.

C. Effect of phase transition on phonons

In the preceding section we have seen that the lattice dynamics of SbSBr is expressed by the central-force model and the sets of eigenvectors given in Fig. 9 are less sensitive to the change of force constants. Since the ions through their vibrations produce electric dipoles in the crystal and these dipoles produce a long-range electric field, their forces make the soft mode A_u^2 unstable. When this mode condenses, the structure is expected to be slightly deformed. That is, Sb and S atoms are displaced relatively to Br atom, which induces static dipole moment along the c axis. The same mechanism of displacements has been observed by Kikuchi *et al.* in SbSI.[18] When the phase transition occurs, the frequencies of the other normal modes are to some extent affected by these displacements.

The phonons shown in Fig. 5, which correspond to B_g^1 and B_g^3 of Fig. 9 receive the effect of the phase transition below 22.8 K. We show in the following that the temperature dependence of these modes is explained by the displacement of Sb and S atoms relative to Br atom below T_c using the results of Sec. V B.

The characteristic features of the modes are described as follows. (1) The energy shift is proportional to the square of the order parameter. (2) These modes become infrared active below T_c. (3) As the modes are transverse-optic (TO), they have no depolarization field. (4) The modes belong to the symmetry different from that of the soft mode, and there is no interaction between them. (5) In our experiment there is no phonon with a temperature-dependent frequency except soft mode and those above. These features indicate that above T_c the Raman-active phonons are nonpolar, so that the transverse and the longitudinal modes are degenerate. In the ferroelectric phase the macroscopic field lifts the degeneracy owing to the disappearance of the inversion symmetry. This splitting is strong in the mode vibrating along the c axis and weak in the mode vibrating perpendicular to the c axis.

Since the frequencies do not change drastically at T_c, we assume that the basis vector in the paraelectric phase is also useful in the ferroelectric phase. In the following, we are interested in the Raman-active mode vibrating along the c axis. Using the normal coordinate W_σ of the normal mode σ, the TO mode of the frequency ω_T, which is described in the paraelectric phase as $\omega_T^2 = R_0$, is written in the ferroelectric phase as

$$\omega_T^2 W_\sigma = R_0 \left[1 + \frac{A U_z^2}{2R_0} + \cdots \right] W_\sigma - Z_\sigma E_{\mathrm{loc}} , \tag{10}$$

where R_0 is the short-range force constant, U_z is the static displacement of atoms which is equal to the order parameter, A is the expansion coefficient, and $A > 0$ is satisfied in the central-force model.[31] W_σ is the linear combination of the displacements of the atoms,

$$W_\sigma = \sum_\alpha M_\alpha^{1/2} c_{\alpha\sigma} U_\alpha . \tag{11}$$

In Eq. (11) the sum is taken over the atoms having mass M_α and displacement U_α. The transformation coefficient ($c_{\alpha\sigma}$) were obtained in Sec. V B. The local field E_{loc} is produced by the "effective charge" Z_σ of the normal mode σ.[32] In our approximation Z_σ is defined as

$$Z_\sigma = \sum_\alpha \frac{e_\alpha c_{\alpha\sigma}}{M_\alpha^{1/2}} , \tag{12}$$

where e_α is the charge on atom α. Apparently Z_σ

of the Raman-active mode is zero above T_c owing to the antiphase motion of the two chains of Sb(3)-S(4)-Br(1) and Sb(4)-S(3)-Br(2). Below T_c Eq. (12) has a nonzero value owing to the static displacement of U_z. Therefore, its magnitude depends on the absolute value of single-chain "effective charge" and its temperature dependence is expressed as

$$Z_\sigma \propto U_z \ . \tag{13}$$

The local field is the linear function of the oscillating polarization and when we assume a simple Lorentz field, it is given by

$$E_{\text{loc}} = \frac{4\pi N}{3V} Z_\sigma W_\sigma \ , \tag{14}$$

where N is the number of primitive unit cells in the crystal volume V. Then Eq. (10) is rewritten as

$$\omega_T^2 = R_0 + (A' - B) U_z^2, \quad A' > 0, \quad B > 0 \ . \tag{15}$$

Equation (15) means that whether ω_T decreases or increases depends on the balance of the two forces but the shift of the frequency is proportional to the square of the order parameter U_z. This is what we see in Fig. 5.

In Eq. (15), the magnitude of the coefficients B is determined by the sum of the single chain in Eq. (12). As seen in Fig. 9, in the B_g^1 mode the positive Sb^{3+} ion [this is an analogy of the ionic model used in SbSI (Ref. 30)] moves in the same direction as the negative S^{2-} and Br^- ions. On the contrary in the B_g^3 mode the positive ion moves in the direction opposite to the two negative ions in a single chain. Therefore, the long-range force of Eq. (14) is strong in the B_g^3 mode but weak in the B_g^1 mode.

Next we consider the frequency change due to the short-range force. We show the elements of the force-constant Jacobian matrix of B_g^1 and B_g^3 in Table IV. This matrix is obtained in the course of the calculation of the frequencies given in Table II. Table IV shows the sensitivity of the frequency to the force constant or the atomic distance change. The mode B_g^1 depends strongly on the force constant or the distance between S(3) and Br(1). Then we expect that when A_u^2 condenses, the frequency of B_g^1 increases overcoming the long-range force. However, B_g^3 is mainly governed by the force constant between Sb(3) and S(4) and is insensitive to the condensation of A_u^2. In this case the frequency of B_g^3 is determined by the long-range force and decreases below T_c.

Within our approximation, the results shown in Fig. 5 furnish evidence to show that the phase transition of SbSBr is the displacive one due to the relative displacement between the Br atom and Sb and S atoms. The same mechanism is also expected in SbSI. We performed the same experiment in SbSI but the phonons near $T_c = 290$ K are so broad that that we could not obtain results which can be equally compared with those of SbSBr. Below 200 K we observed this tendency but the temperature dependence of the phonon was small. The tendency of these peak shifts was observed in Ref. 17. The authors, however, did not pay attention to the following fact. The frequency of $\Gamma_2(R)$ (in our notation B_{2g} or B_{3g}) shifts from 37 cm^{-1} at 35 °C to 51 cm^{-1} at -70 °C, while the frequency of another $\Gamma_2(R)$ shifts from 215 to 206 cm^{-1}.

TABLE IV. Jacobian matrix for the force constants of B_g^1 and B_g^3 modes [$\text{cm}^{-2}/(10^4$ dyn/cm)].

	B_g^1	B_g^3
$F_{\text{Sb(3)-Br(1)}}$	19.7	25.0
$F_{\text{Sb(3)-S(4)}}$	0.7	84.2
$F_{\text{Sb(3)-S(3)}}$	0	0
$F_{\text{S(3)-Br(1)}}$	45.0	48.6
$F_{\text{Sb(3)-Sb(4)}}$	18.8	22.1

VI. SUMMARY

We have studied the Raman spectra of SbSBr grown by a vapor transport method in both para- and ferroelectric phases. A strong soft mode with A_1 symmetry appears below 22.8 K. From the temperature dependence of its frequency, the scattering intensity, and its linewidth, the transition is determined to be a displacive one close to the tricritical point. Owing to its low phase-transition temperature and its transparency to the He-Ne laser line, we made clear the changes of the lattice modes accompanied with the phase transition. It turned out that the simplified unit-cell model usually applied to SbSI is not appropriate and the full space group D_{2h}^{16} (four molecules) is necessary to interpret the Raman spectra. In the analysis of our Raman spectra there is no contradiction to the assumption that the ferroelectric phase is C_{2v}^9. The phonons having A_1 and A_2 symmetries are Davydov pairs having an interaction energy of about 60 cm^{-1}. This energy is also expected between the phonons having B_1 and B_2 symmetries. The soft-mode frequency shifts with temperature having an exponent of 0.23. It is discussed that this value is close to the critical exponent of the order parameter. The intensity of the soft mode decreases as the temperature approaches

T_c. This phenomenon is discussed in connection with existing theories. Two B_1 or B_2 modes are affected by the phase transition and shift in the opposite directions by 4 cm^{-1} below T_c. Their shifts are nearly proportional to the square of the order parameter.

Based on the correlation of the normal modes between para- and ferroelectric phases, we proposed a model of the lattice dynamics. In the model we take into account the interaction between the double chains as Davydov splitting and the intrachain interaction was described in the bond-stretching forces shown in Fig. 8. It was shown that it is possible to calculate the phonon frequencies and the set of eigenvectors from the model. The anomalous shifts of two B_2 or B_3 modes below T_c are considered in this model and we conclude that the shift is the result of relative displacement of Sb and S atoms to Br atom along the c axis below T_c, which is expected from the condensation of the ferroelectric mode in our model.

ACKNOWLEDGMENTS

The authors wish to thank Dr. T. Sekine for useful discussions, and Professor R. Yoshizaki for valuable technical support. This work is partially supported by the Grant-in-Aid for Scientific Research from the Ministry of Education which is deeply appreciated.

---

[1] G. D. Christofferson and J. D. McCullough, Acta Crystallogr. 12, 14 (1959).

[2] R. Nitzsche and W. J. Merz, J. Phys. Chem. Solids 13, 154 (1960).

[3] K. Ohi, J. Phys. Soc. Jpn. 25, 1369 (1968).

[4] R. Nitzsche, H. Roetschi, and P. Wild, Appl. Phys. Lett. 4, 210 (1964).

[5] T. A. Pikka and V. M. Fridkin, Fiz. Tverd. Tela (Leningrad) 10, 3378 (1968) [Sov. Phys.—Solid State 10, 2668 (1969)].

[6] K. Ishikawa, Y. Shikata, and K. Toyoda, Phys. Status Solidi A 25, K187 (1976).

[7] E. Furman, O. Brafman, and J. Makovsky, Phys. Rev. B 13, 1703 (1976).

[8] T. Tatsuzaki, K. Itoh, S. Ueda, and Y. Shindo, Phys. Rev. Lett. 17, 198 (1966).

[9] K. Uchinokura, T. Inushima, E. Matsuura, and A. Okamoto, Ferroelectrics 38, 901 (1981).

[10] E. Furman, O. Brafman, and J. Makovsky, Phys. Rev. B 8, 2341 (1973).

[11] T. Inushima, A. Okamoto, K. Uchinokura, and E. Matsuura, J. Phys. Soc. Jpn. 48, 2167 (1980).

[12] T. Inushima, K. Uchinokura, E. Matsuura, and A. Okamoto, in *Proceedings of the Fifteenth International Conference on the Physics of Semiconductors,* edited by S. Tanaka and Y. Toyozawa (Physical Society of Japan, Tokyo, 1980); J. Phys. Soc. Jpn. 49, Suppl. A, 753 (1980).

[13] From the observation of the coexistence of the para- and ferroelectric phases at T_c, the transition was determined to be first order close to the tricritical point. We will report on this in another paper.

[14] M. E. Lines and A. M. Glass, *Principles and Applications of Ferroelectrics and Related Materials* (Clarendon, Oxford, 1977).

[15] T. Inushima, K. Uchinokura, K. Sasahara, E. Matsuura, and R. Yoshizaki, Ferroelectrics 38, 885 (1981).

[16] D. K. Agrawal and C. H. Perry, Phys. Rev. B 4, 1893 (1971).

[17] M. Balkanski, M. K. Teng, S. M. Shapiro, and M. K. Ziolkiewicz, Phys. Status Solidi B 44, 355 (1971).

[18] A. Kikuchi, Y. Oka, and E. Sawaguchi, J. Phys. Soc. Jpn. 23, 337 (1967).

[19] R. Loudon, Adv. Phys. 13, 423 (1964).

[20] R. Blinc, M. Mali, and A. Novak, Solid State Commun. 6, 327 (1968).

[21] The subscript of the atom position follows the one of Ref. 18 or Ref. 7 instead of Ref. 1. See also Fig. 8.

[22] M. K. Teng, M. Balkanski, M. Massot, and M. K. Ziolkiewicz, Phys. Status Solidi B 62, 173 (1974).

[23] J. Petzelt, Phys. Status Solidi 36, 321 (1969).

[24] E. F. Steigmeier and H. Auderset, Solid State Commun. 12, 565 (1973).

[25] T. Schneider and E. Stoll, Phys. Rev. B 13, 1216 (1976).

[26] R. A. Cowley, Adv. Phys. 12, 421 (1963).

[27] T. J. Wieting, A. Grisel, F. Levy, and Ph. Schmid, in *Quasi-One-Dimensional Conductors I,* Vol. 95 of *Lecture Notes in Physics,* edited by S. Barisic (Springer, Berlin, 1979), p. 354.

[28] R. Zallen, in *Proceedings of the Twelfth International Conference on the Physics of Semiconductors,* edited by M. K. Kuhn (B. G. Teubner, Stuttgart, 1974), p. 251.

[29] D. E. Mann, T. Shimanouchi, J. H. Meal, and L. Fano, J. Chem. Phys. 27, 43 (1957).

[30] K. Nakao and M. Balkanski, Phys. Rev. B 8, 5759 (1973).

[31] W. Cochran, Adv. Phys. 9, 387 (1960).

[32] W. Hayes and R. Loudon, *Scattering of Light by Crystals* (Wiley, New York, 1978), p. 150.